Med Bio Eng Comput (2006) 44:971-982
DOI 10.1007/s11517-006-0113-6

ORIGINAL ARTICLE

Theoretical modeling of micro-scale biological phenomena in human coronary arteries

Kelvin Wong · Jagannath Mazumdar · Brandon Pincombe · Stephen G. Worthley · Prashanthan Sanders · Derek Abbott

Received: 28 November 2005 / Accepted: 14 September 2006 / Published online: 18 October 2006

Abstract This paper presents a mathematical model of biological structures in relation to coronary arteries with atherosclerosis. A set of equations has been derived to compute blood flow through these transport vessels with variable axial and radial geometries. Three-dimensional reconstructions of diseased arteries from cadavers have shown that atherosclerotic lesions spiral through the artery. The theoretical framework is able to explain the phenomenon of lesion distribution in a helical pattern by examining the structural parameters that affect the flow resistance and wall shear stress. The study is useful for connecting the relationship between the arterial wall geometries and hemodynamics of blood. It provides a simple, elegant and non-invasive method to predict flow properties for geometrically complex pathology at micro-scale levels and with low computational cost.

K. Wong (✉) · J. Mazumdar · D. Abbott
Centre for Biomedical Engineering (CBME)
and School of Electrical & Electronic Engineering,
The University of Adelaide, Adelaide, SA 5005, Australia
e-mail: kwong@eleceng.adelaide.edu.au

S. G. Worthley · P. Sanders
Cardiovascular Research Centre,
Department of Cardiology, Royal Adelaide Hospital
and the Discipline of Medicine, University of Adelaide,
Adelaide, SA 5005, Australia

B. Pincombe
Land Operations Division, Defence Science
and Technology Organisation, P.O. Box 1500,
Edinburgh, SA 5111, Australia

Keywords Atherosclerosis · Axial and radial asymmetry · Spiraling lesion · Resistance to flow ratio · Wall shear stress

1 Introduction

Atherosclerosis is a major underlying cause of angina and myocardial infarction [12]. In atherosclerotic arteries, the lumen is typically narrowed and the wall is stiffened by the build up of plaque with a lipid core and a fibromuscular cap [11]. In some cases the arterial wall can remodel itself by increasing its external diameter to accommodate a plaque without narrowing the lumen, producing angiographically silent plaques detectable only by intravascular ultrasound [17]. In the majority of cases where this does not occur the resulting stenosis reduces blood flow to some degree. Atherosclerotic stenoses are the main cause of stable angina [10]. Plaque rupture can lead to the formation of a thrombus that blocks blood flow to the heart leading to unstable angina or myocardial infarction [11]. Plaques with large atheromatous cores, thin fibromuscular caps and inflamed caps are particularly vulnerable [12] regardless of the degree of stenosis [23]. There is some speculation that wall shear stress leads to luminal thinning and promotes plaque rupture [5, 16, 45] although there are also questions about whether high hemodynamic shear alone would disrupt a stenotic plaque [12, 15] as hemodynamic stresses are usually much smaller than mechanical stresses imposed by blood and pulse pressures [22]. Fast and accurate estimation of the reduction in flow due to stenoses is important in determining their effects on angina [20, 34] and accurate estimation of the increase in wall

shear stress due to stenoses has implications for the theory of plaque rupture [12]. In particular, discussions in the presence of more realistic wall geometries are needed [30].

The preferred surgical intervention for atherosclerosis, balloon angioplasty, is quick and involves minimal risk. A small catheter with an inflatable balloon is inserted into the femoral artery and guided to the stenosis by angiography. Inflation of the balloon crushes the stenosis. Healing entails proliferation of smooth muscle cells followed by the deposition of new collagen [10] thus thickening the cap and reducing the risk of thrombus formation, as well as pushing the plaque into the wall thereby increasing blood flow. A Poiseuille flow model [20, 34] is typically used by the radiographer to aid the cardiologist in deciding whether to crush a given stenosis. While Newtonian models, such as Poiseuille flow, are appropriate for determining flow after an intervention [4] they are inappropriate in arteries narrower than 0.5 mm and are questionable in those smaller than 0.8 mm [31] as blood displays a marked shear-dependent viscosity [9] and a finite yield stress may be necessary before the flow can commence [2]. Although the major coronary arteries can be as wide as 4 mm, clinically significant stenoses for angina typically reduce the diameter of the artery by 85% or more, and so stenosed coronary arteries are rarely wider than 0.5 mm at their narrowest [28]. Power law [31, 37], Bingham [29], Herschel-Bulkley [8] and Casson [25, 30, 37] equations have been suggested as models of this situation. While the Casson model is the most realistic of these [3, 26], the power law model is the simplest and requires the least number of numerical integrations to achieve a solution [31]. The Casson model predicts more reduction in flow than Newtonian alternatives. The power law model consistently predicts slightly more reduction in flow than the Casson model [3] and thus errs, very slightly, on the side of caution. For applications such as angiographic assessment of stenoses, the power law model has the advantages of speed and ease of solution.

High-resolution imaging techniques have been used to document the geography of atherosclerosis within the arterial tree. These imaging technologies include intravascular ultrasound, multi-detector computerized tomography and magnetic resonance imaging. The last of these technologies, magnetic resonance imaging, is a non-invasive technology that does not require radiation, and affords the greatest intrinsic contrast between soft tissue structures. In particular, it has been shown to accurately document atherosclerotic plaque composition [41] and arterial wall remodeling [42]. Descriptions of geometric models using numerical mesh constructed from magnetic resonance images have been used to calculate wall shear stresses for example [19, 38]. However, still limitations exist with the spatial and temporal resolution of magnetic resonance imaging in performing this analysis in human coronary arteries [43]. Therefore, there is still much to be gained from advanced mathematical modeling algorithms assessing the atherosclerotic vessel wall.

Lack of solutions in the presence of realistic wall geometries has reduced the applicability of non-CFD based mathematical modeling techniques to blood flow through stenosed arteries [1, 30]. Symmetry has been assumed in past work [29] even though atherosclerotic plaques in the coronary arteries are typically longitudinally and radially asymmetric. Furthermore, helical atherosclerotic plaques have been detected in human left anterior descending coronary arteries [14] and such helical plaques have been linked to hemodynamic factors in the femoral arteries [39]. We extend previous work modeling the circumferential and longitudinal variation of lesions [40] to more accurately model the wall geometry and to consider helical plaque structures. By varying the properties of the lesion, such as the diseased height, axial and radial shape parameters, as well as the degree of lesion spiral that develops onto the inner wall of the atherosclerotic artery, the mathematical model is able to relate the subintimal helical distribution of lesions to flow resistance and shear stress on the arterial wall for straight arteries. The requirement of straightness over such a length limits the applicability of this work to the coronary arteries but, more generally, the reduction in flow and the wall shear stress ratios are found for blood flow modeled by a power law fluid through a variety of complicated stenosis geometries.

2 Definition of the arterial wall geometry

The development of a mathematical model of blood flow in arterial vessels established an important framework in the analytical solution of non-Newtonian flow through stenosed vessels and aneurysms, elastic and viscoelastic tubes [44]. Solution of the approximate equations governing steady flow through stenosed arteries has been presented [21]. Detailed treatment of non-Newtonian models of blood flow through rigid and elastic walled arteries have been examined using the power law model [27, 31, 32].

Although the arterial wall profiles used in such studies are considered to be rigid and highly simplified, and do not reflect the true mechanical and geometrical characteristics of the typical atherosclerotic artery, it

does not hinder the ability of the model to predict the response for flow resistance ratio under the influence of an aneurysm or stenosis at different degrees of atherosclerosis. A high resolution profile of a realistic arterial segment will only add excessive shape parameters to the mathematical derivation of flow properties in the examined arterial segment by incorporating redundant geometrical features in its profile expression. The analytical shape that approximates a low resolution of the experimentally determined profile can be adopted effectively for analytical study of blood flow in vitro as it is able to generate the variation profile of the flow resistance ratio with respect to arterial dimensional modifications.

The configuration of an arterial segment is an important determinant in characterizing the nature of blood flow through it. For a three-dimensional artery, the wall geometry can be either symmetrical or asymmetrical in the axial and radial directions. Axial symmetry implies that for a typical lesion distribution that varies longitudinally, there exists a plane of symmetry for the arterial surface such that it dissects the varying wall profile along the examined segment from the proximal to distal end of the artery, and through the axis of the vessel. We define radial asymmetry to be non-uniformity in the distribution along the circumference of the artery. The geometry of the artery can be presented using a series of sagittal and coronal planes.

2.1 Axial and radial symmetry

Figure 1 shows the longitudinal distribution of a segment for an idealized blood vessel structure. The axial geometry is determined by the diseased wall height δ, shape parameter of diseased wall segment s_z for an atherosclerotic lesion of length l through an artery originally of radius R_0. Variation of s_z forms the lesion profile given by the solid, dash and dotted protrusion outlines. Here, α is the distance from the origin to the start of the diseased portion and β is the distance from the origin to the end of it. The wall equations allow both constriction (stenosis) and dilation (aneurysm) of the lumen.

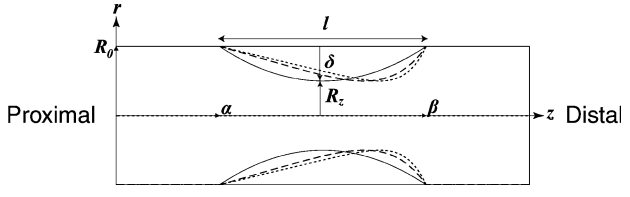

Fig. 1 Axial variation of arterial wall with lesion development in the $(r - z)$ plane. A single lesion segment is presented from the proximal to the distal end for the case of stenosis. An aneurysm can be constructed by negating the value of diseased wall height δ. An ideal artery is presented and variation of s_z causes the stenosis or aneurysm to be skewed asymmetrically along the z-axis

The axial geometry $g_z(z)$ of the diseased segment is defined as

$$g_z(z) = \begin{cases} \delta f_1(z) & \text{for } \alpha \le z \le \beta \\ 0 & \text{otherwise} \end{cases}, \tag{1}$$

and

$$f_1(z) = \frac{1}{l^{s_z} s_z - 1} s_z^{\frac{s_z}{s_z - 1}} [l^{s_z - 1}(z - \alpha) - (z - \alpha)^{s_z}] \quad \text{for } s_z \ge 2. \tag{2}$$

It can be observed that the geometrical wall height variation is dependent on the axial segmental distance z that is taken from α onwards, and is limited by a length of β. The expression of $f_1(z)$ can be constructed using the components $(z–\alpha)$ and $(z - \alpha)^{s_z}$.These two terms are normalized after dividing each of them by l and l^{s_z} respectively. The difference of the two terms is multiplied by a function of the shape parameter, s_z. Therefore $f_1(z)$ is dimensionless and represents the normalized height of the diseased segment.

Given that the normalized diseased height with respect to a healthy arterial radius is:

$$\Delta(\delta) = \frac{\delta}{R_0} \quad \text{for} - R_0 \le \delta \le R_0, \tag{3}$$

the equation describing the geometry of the wall after normalization is:

$$\frac{R_z}{R_0} = \begin{cases} 1 - \Delta(\delta) f_1(z) & \text{for } \alpha \le z \le \beta \\ 1 & \text{otherwise} \end{cases}, \tag{4}$$

where s_z is a parameter determining the shape of the stenosis, and R_z is the general radius of the artery. The lesion is asymmetrically profiled about the diseased center for $s_z > 2$.

2.2 Axial symmetry and radial asymmetry

The equations governing the wall profile for both longitudinal and radial orientations give a better representation of a realistic arterial segment. Useful deductions on the flow properties through three-dimensional varying wall profiles and arterial configuration can be established. We examine the variation of diseased wall height, shape of diseased wall segment

and number of diseased segments that are determined by the parameters δ, s_θ and k_θ respectively.

A circumferential profile $f_2(\theta)$ modifies arterial wall in the radial plane. Increasing the shape parameter s_θ will result in a higher variation for the circumferential distribution of atherosclerotic lesion. Figure 2 illustrates three atherosclerotic profiles superimposed on the same coronal plane, whereby $k_\theta = 2$ and with shape parameters such that $s_\theta{}^{(3)} > s_\theta{}^{(2)} > s_\theta{}^{(1)}$. The flow solution for this geometry is valid only if s_θ is non-zero. It should be discrete and non-negative for $k_\theta > 1$, but it can be continuous when $k_\theta = 1$. Given that

$$f_2(\theta) = \sin^{2s_\theta}\left(\frac{k_\theta}{2}\right)\theta \quad \text{where } s_\theta \geq 1 \text{ for } k_\theta \geq 1, \tag{5}$$

we see the diseased geometry varies asymmetrically about the origin of the stenosis, and so dilation both longitudinally and circumferentially is given by:

$$g_{z,\theta}(z,\theta) = g_z(z) f_2(\theta) \quad \text{for } \alpha \leq z \leq \beta, 0 \leq \theta \leq 2\pi. \tag{6}$$

The general radius of the artery that varies along the z-axis and $(r - \theta)$ plane is denoted by R_z. This geometry represents an artery that has uneven diseased segments in the radial plane and asymmetrical axial geometry about the center of the origin of the lesion. The normalized wall height ratio equation that describes the geometry of the vessel, by having this radial dimension as a parameter, is now defined as

$$\frac{R_{z,\theta}}{R_0} = \begin{cases} 1 - \Delta(\delta) f_1(z) f_2(\theta) & \text{for } \alpha \leq z \leq \beta \\ 1 & \text{otherwise} \end{cases}. \tag{7}$$

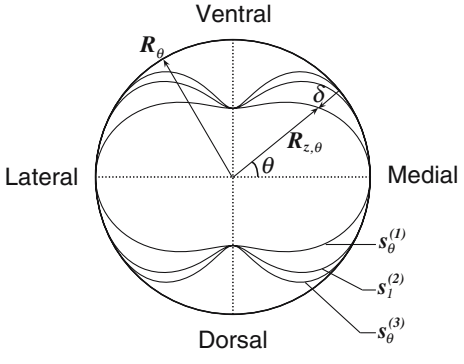

Fig. 2 Radial variation of arterial wall due to presence of localized lesions in the $(r - \theta)$ plane. The shape and number of localized lesions can be controlled by parameters δ, s_θ and k_θ to construct the idealized lumen that is similar to the real arterial structure. Nevertheless, there will always be a limitation in the complicated shape variation, which is controlled by these designated parameters

2.3 Axial and radial asymmetry

A helical lesion can be modeled by introducing a variable angular phase shift allowing the peak of the stenosis to relocate along the circumference of the arterial wall in the coronal plane. In order to simplify modeling the maximum height, δ, of the stenosis is kept constant throughout the spiral. The angular phase shift, ϕ, is dependent on the axial dimension. The lesion profile is non-uniform at every sagittal and coronal plane as seen in Fig. 3.

The parameters that control the geometry of a single lesion spiraling structure are the diseased height δ, the radial shape parameter s_θ, the degree of spiral ψ, the length of wall it extends along l and radius of the healthy artery R_0. For constant radial variation, the lesion geometry is given by:

$$g_z(z) = \begin{cases} \delta & \text{for } \alpha \leq z \leq \beta \\ 0 & \text{otherwise} \end{cases}. \tag{8}$$

The variable magnitude of spiral, ψ, that is quantified in degrees, measures the number of helical coils for a specific arterial length l. A spiraling lesion can be defined by:

$$g_{z,\theta}(z,\theta) = g_z(z) f_3(\theta, z) \quad \text{for } \alpha \leq z \leq \beta,\ 0 \leq \theta \leq 2\pi, \tag{9}$$

where

$$f_3(z,\theta) = \sin^{2s_\theta}\left(\frac{k_\theta}{2}\right)(\theta + \phi) \quad \text{for } s_\theta \geq 1, k_\theta \geq 1, \tag{10}$$

and

$$\phi = \psi\frac{z}{l} \quad \text{for } \psi \geq 0. \tag{11}$$

An artery with longitudinally uniform and radially asymmetrical diseased segments is represented by:

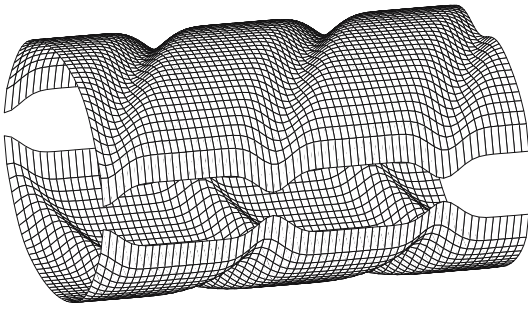

Fig. 3 Mesh of diseased artery that is split into two halves exposing the spiraling of a single lesion along the arterial wall. The degree of spiral is an indicator for the number of turns along an arterial length. Cases of such spiraling lesion are found in diseased arteries of cadavers [39]

$$\frac{R_{z,\theta}}{R_0} = \begin{cases} 1 - \Delta(\delta) f_3(z,\theta) & \text{for } \alpha \le z \le \beta \\ 1 & \text{otherwise} \end{cases}. \quad (12)$$

3 Theoretical models of blood flow

In a fluid flow that is incompressible and under a steady flow field, the shear rate of strain of a material fluid element is defined as the rate of decrease of the angle formed by two mutually perpendicular lines on the element. As such, the shear strain rate $\dot{\gamma}$ is defined as a function of τ and is proportional to the rate of decrease of axial velocity, v_z along the arterial radius:

$$\dot{\gamma} = f(\tau) = -\frac{\mathrm{d}v_z}{\mathrm{d}r}. \quad (13)$$

In general, the shear strain rate can be defined as a function of τ and the mechanical characteristics of the flow can be described by the Poiseuille's law model [33], which defines a linear relationship between the shear stress and strain components with the viscosity as its gradient. The model can be expressed mathematically as

$$\tau = \mu\dot{\gamma}. \quad (14)$$

The power law or Ostwald de-Waele model includes the flow behavior index to introduce the non-Newtonian effect to the fluid. In this regard, a Newtonian fluid can be described by a Poiseuille flow since it conforms to the Newton's law of viscosity. It defines the flow properties based on a type of time independent non-Newtonian fluid [24] with shear dependent viscosity. Given that τ is the shear stress, $\dot{\gamma}$ is the shear strain rate, m is the consistency and n is the flow behavior index. The model can be expressed by the constitutive equation:

$$\tau = m\dot{\gamma}^n. \quad (15)$$

For pseudo plastic fluids such as blood, $n < 1$, the apparent viscosity decreases as the shear strain rate increases. The power law model reduces to its Newtonian case when $n = 1$ and $m = \mu$, which is the viscosity of the fluid.

Other versions of non-Newtonian fluids exist in literature, such as the Herschel-Bulkey [18], Bingham [6] and Casson [7] models, which introduce an additional yield stress τ_0 at zero shear rate to the power law or Poiseuille models, such that $\tau \ge \tau_0$ in order for flow to take place. A Bingham fluid resembles a Herschel-Bulkey model, but it establishes a linear relationship between shear stress and shear strain rate. A Casson model takes the form of the Bingham model, but it effects an exponential of $\frac{1}{2}$ for every term in its equation. In summary, the following equations describe each of these fluids, Bingham fluid:

$$\tau = \mu\dot{\gamma} + \tau_0 \quad \text{for } \tau \ge \tau_0, \dot{\gamma} = 0 \quad \text{for } \tau \le \tau_0. \quad (16)$$

Herschel-Bulkey fluid:

$$\tau = \mu\dot{\gamma}^n + \tau_0 \quad \text{for } \tau \ge \tau_0, \dot{\gamma} = 0 \quad \text{for } \tau \le \tau_0. \quad (17)$$

Casson fluid:

$$\tau = (\mu^{\frac{1}{2}}\dot{\gamma}^{\frac{1}{2}} + \tau_0^{\frac{1}{2}})^2 \quad \text{for } \tau \ge \tau_0, \dot{\gamma} = 0 \quad \text{for } \tau \le \tau_0. \quad (18)$$

The application of these fluid models for the study of flow resistance in atherosclerotic arteries has been examined thoroughly in the literature [27, 31, 32]. The flow resistance ratio for each of these models vis-à-vis variation of arterial geometry typically gives the same direction of increment or response change, but at different magnitudes. Although the Casson model has been shown to be the most appropriate physical description of blood flow in vitro [26], it is more complicated mathematically as compared to the power law model. The assumption of a yield stress term and the square root of each of the parameters in the equation makes the solution difficult in any realistic wall geometry [29]. The power law model consistently predicts slightly greater reduction in flow than the Casson model [3], which itself predicts greater reduction in flow than Newtonian alternatives. Therefore, it is likely to slightly overestimate the flow resistance, but is effective as a mathematical entity in the theory for connecting the flow properties with the geometrical characteristics of the arterial profile.

4 Mechanics of flow through an artery with axially and radially varying wall geometry

Accurate estimation of the reduction in blood flow caused by a stenosis is clinically important when deciding whether to intervene [29] and careful approximation of the increase in wall shear stress has implications in the theory of plaque rupture and thrombus formation [5, 16, 45]. The resistance to flow ratio is the blood flux through the stenosed or dilated artery with respect to that through a healthy artery.

The wall shear stress ratio compares the maximum shear stress on the wall of the plaque with that which will be present on the wall of the artery if there is no plaque. In both cases ratios are determined both because they give important information of the effect of the stenosis and because they obviate the need for exact calculations of difficult to calculate quantities through cancellation.

4.1 Derivation of flow resistance

To work out the ratio of flux through a stenosed artery to that through its healthy equivalent it is first necessary to derive expressions for the flux in these two cases. The flux, Q, through the artery [13, 24] is:

$$Q = \int_0^{2\pi} \int_0^{R_{z,\theta}} r v_z \mathrm{d}r \mathrm{d}\theta. \tag{19}$$

Using integration by parts, $Q = \int_0^{R_{z,\theta}} r v_z \mathrm{d}r$ can be expressed in terms of r and $\frac{\mathrm{d}v_z}{\mathrm{d}r}$ and by applying no-slip boundary condition, $v_z = 0$ when $r = R_{z,\theta}$:

$$Q = \frac{1}{2} \int_0^{2\pi} \int_0^{R_{z,\theta}} r^2 f(\tau) \mathrm{d}r \mathrm{d}\theta. \tag{20}$$

Now τ is given by:

$$\tau(r) = -\frac{r}{2}\frac{\mathrm{d}p}{\mathrm{d}z}, \tag{21}$$

where p is the pressure. Therefore, the value of τ at $r = R_{z,\theta}$ is given by

$$\tau_R = \tau(R_{z,\theta}) = -\frac{R_{z,\theta}\mathrm{d}p}{2\ \mathrm{d}z}. \tag{22}$$

Re-expression of the integration in (20) and using Eqs. 21 and 22 yields:

$$Q = \frac{1}{2} \int_0^{2\pi} {R_{z,\theta}}^3 \frac{1}{{\tau_R}^3} \int_0^{\tau_R} \tau^2 f(\tau) \mathrm{d}\tau \mathrm{d}\theta, \tag{23}$$

where the plasma layer is assumed to be negligible and τ_R is the shear stress at the wall. Substitution of Eqs. 13 and 14 into 23, and integration by τ gives

$$Q = \left(\frac{1}{m}\right)^{\frac{1}{n}} \frac{1}{2} \int_0^{2\pi} {R_{z,\theta}}^3 \frac{1}{{\tau_R}^3} \left[\frac{n}{3n+1} \tau^{\frac{3n+1}{n}}\right]_0^{\tau_R} \mathrm{d}\theta. \tag{24}$$

Rearranging,

$$Q = \left(\frac{1}{m}\right)^{\frac{1}{n}} \frac{n}{2(3n+1)} \int_0^{2\pi} {R_{z,\theta}}^3 \tau_R^{\frac{1}{n}} \mathrm{d}\theta. \tag{25}$$

Further substitution of Eq. 22 into 25 gives

$$Q = \left(\frac{1}{m}\right)^{\frac{1}{n}} \frac{n}{2^{1+\frac{1}{n}}(3n+1)} \left(-\frac{\mathrm{d}p}{\mathrm{d}z}\right)^{\frac{1}{n}} \int_0^{2\pi} {R_{z,\theta}}^{3+\frac{1}{n}} \mathrm{d}\theta. \tag{26}$$

Integration of Eq. 26 with respect to z such that the pressure difference, $\Delta P = p_i - p_0$,and setting the conditions that $p = p_i$ at $z = 0$ and $p = p_0$ at $z = l$ gives

$$\Delta P = \frac{2^{n+1}(3n+1)^n m Q^n}{n^n {R_0}^{3n+1}} \int_0^l \frac{\mathrm{d}z}{\left[\int_0^{2\pi} \left(\frac{R_{z,\theta}}{R_0}\right)^{3+\frac{1}{n}} \mathrm{d}\theta\right]^n}. \tag{27}$$

Flow resistance is given by:

$$\lambda = \frac{\Delta P}{Q}. \tag{28}$$

Division of flow resistance for an abnormal artery with a normal one yields the flow resistance ratio for flow through a longitudinal and radial varying artery in the coronal and sagittal planes as shown:

$$\overline{\lambda}(z,\theta) = \frac{2\pi^n}{l} \int_0^l \frac{\mathrm{d}z}{\left[\int_0^{2\pi} \left(\frac{R_{z,\theta}}{R_0}\right)^{3+\frac{1}{n}} d\theta\right]^n}, \tag{29}$$

and for uniform radial distribution,

$$\overline{\lambda}(z) = \frac{1}{l} \int_0^l \frac{\mathrm{d}z}{\left(\frac{R_z}{R_0}\right)^{3n+1}}. \tag{30}$$

For a normal artery, $R_{z,\theta} = R_0$ and this gives a flow resistance ratio of one. For a fully occluded artery $R_{z,\theta} = 0$ and the flow resistance is infinite.

4.2 Derivation for wall shear stress

From Eq. 24 it can be determined that the axial wall shear stress on an axially and radially variable stenosis is:

$$\tau_R(z,\theta) = m\left[\frac{2(3n+1)}{n}\right]^n \frac{1}{\left[\int_0^{2\pi} {R_{z,\theta}}^3 \mathrm{d}\theta\right]^n}. \tag{31}$$

For a normal artery the axial wall shear stress is:

$$\tau_N = \frac{m}{{R_0}^{3n}}\left[\frac{(3n+1)}{n\pi}\right]^n. \tag{32}$$

The wall shear stress ratio of an axial and radial varying diseased artery to that of a normal one in the axial direction is given by:

$$\overline{\tau}(z,\theta) = \frac{\tau_R(z,\theta)}{\tau_N} = \left[\frac{2\pi}{\int_0^{2\pi}\left(\frac{R_{z,\theta}}{R_0}\right)^3 \mathrm{d}\theta}\right]^n. \tag{33}$$

For a uniform radial distribution,

$$\overline{\tau}(z) = \frac{\tau_R(z)}{\tau_N} = \frac{1}{\left(\frac{R_z}{R_0}\right)^{3n}}. \tag{34}$$

5 Results

In this section, the degree and configuration of atherosclerosis is varied to understand the relationship between the arterial geometry and blood flow resistance. Useful deductions on the geometrical variation and its effect on the hemodynamics of blood are presented. The study examines, in particular, how the axial and radial variability of arterial wall geometry can be combined to affect the blood flow resistance in a single isolated vessel. The model is able to predict the degree of aggravation in occluded arteries vis-à-vis development of atherosclerotic spiraling lesion.

5.1 Variation of axial and radial wall geometries

The arterial geometry with variable diseased height and shape in the circumferential and longitudinal orientations is determined by δ, s_θ and k_θ in the radial $(r-\theta)$ plane and δ and s_z in the axial $(r-z)$ plane.

Figure 4 describes lesions of various shapes that is determined by s_θ from 1 to 8, and for two configurations ($k_\theta = 1$ and 2) in the radial plane. The plots demonstrate that as the value of s_θ increases, the diseased regions become more compact toward the origin of the lesion. When s_θ is zero, the distribution of lesion on the circumference of the artery is uniform.

Figure 5 shows the plots of lesions in the axial plane that have shape parameter s_z at 2, 5 and 15 for each subfigure. The geometrical profile of the lesion changes for a different value of s_z. δ is varied from – 0.1125 to 0.1125 mm at intervals of 0.0225 mm and the resulting wall profiles are plotted in solid lines. The healthy arterial wall is displayed using dotted lines. R_0 and l are standardized at 0.45 and 7.5 mm respectively.

We construct an axially and radially varying artery (in Fig. 6) such that only one diseased segment is considered. Here, $\alpha = 0$, $l = 7.5$ mm, $R_0 = 0.45$ mm. The intermediate wall heights δ vary from – 0.25 to 0.25 mm and are illustrated with dotted profiles. This diagram presents an axial and radial asymmetrical artery whereby $k_\theta = 1$. The radial shape parameter is defined to be $s_\theta = 8$. The axial profile is non-uniform and set at $s_z = 2$.

The surface curves for the resistance to flow ratio $\overline{\lambda}$ responding to effect of δ, s_z, s_θ and k_θ can be plotted and analyzed. The flow is assumed to be Newtonian. (i.e., $n = 1$). The integration with respect to θ is evaluated analytically and then raised to the power of n. The reciprocal of the resulting expression with respect to z is integrated numerically to calculate the flow resistance. The geometry of diseased segments in the radial and axial orientation of the artery has been defined and the variation of the parameters δ, s_z, s_θ and k_θ are investigated for their effect on the flow resistance.

From Fig. 7a, the change of flow resistance ratio, $\overline{\lambda}$, with respect to s_θ is smaller when the diseased wall height is constant at $\Delta = -0.5$ (aneurysm) as compared to when it is fixed at $\Delta = 0.5$ (stenosis). When an arterial dilation is present, $\overline{\lambda}$ decreases with respect to s_θ but with a much larger gradient in comparison. There is no variation for $\overline{\lambda}$ versus s_θ when $\Delta = 0$. This is theoretically correct as the shape parameter has no effect on a healthy normal artery. At low values of s_θ, the acceleration of $\overline{\lambda}$ with respect to Δ is higher than when s_θ is set at high values. The graph for flow resistance is generated for grid of $[s_\theta \times s_z]$ in Fig. 7b, whereby s_z is varied from 2 to 82 at intervals of 8. This shows that the value of flow resistance ratio is higher for smaller values of radial and axial shape parameters, s_θ and s_z, and that the deceleration of $\overline{\lambda}$ is reduced when flow is monitored in the range of high shape parameters $[s_\theta \times s_z]$ variation.

A stenosis of the artery is characteristically followed by dilation due to the sudden increase in pressure of the blood immediately after flowing through the narrowing of the vessel [35]. Equation 28 defines the flow resistance ratio to be proportional to the pressure difference across the stenosis. We explain the formation of vessel dilation immediately after a stenosis by relating the sudden release of blood pressure build up after passing through an occlusion. Since the pressure is related to the momentum of fluid transport, a high concentration of 'formed' elements suspended in the plasma such as erythrocytes, leukocytes and platelets

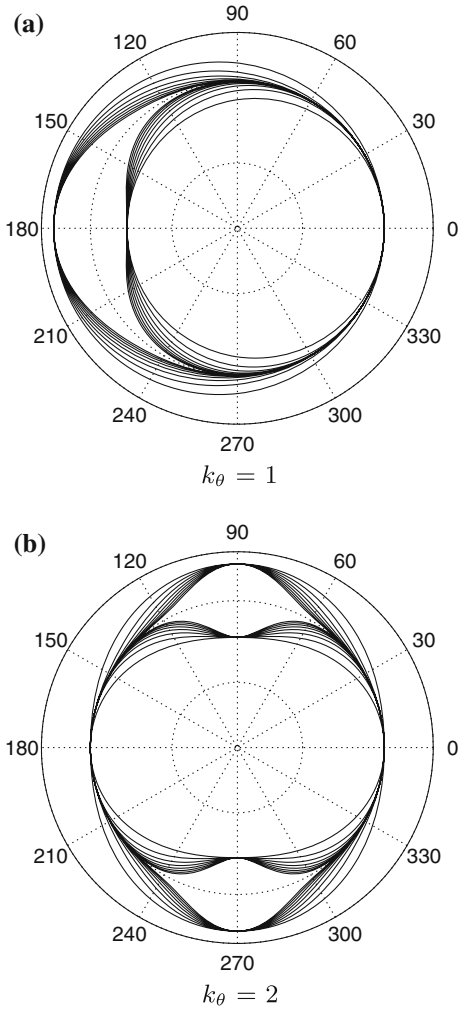

Fig. 4 Plot of arterial profile in the radial plane that is determined by diseased wall height δ, shape of diseased wall segment s_θ and number of localized lesion k_θ, by varying s_θ in the range 1–8 at intervals of 1, and fixing $\Delta = [-0.25, +0.25]$ and $k_\theta = [1, 2]$. The variable control of the lumen geometry can be achieved as such

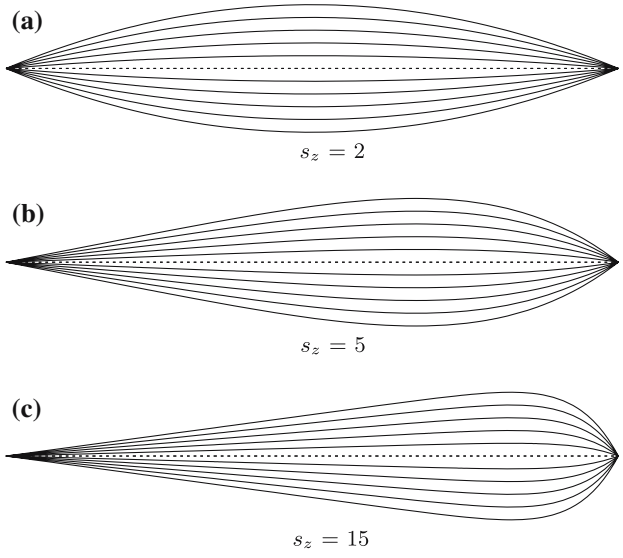

Fig. 5 Plot of arterial profile in the axial plane that is determined by diseased wall height δ, shape of diseased wall segment s_z and the length of localized lesion l. The normalized diseased wall height Δ is varied from – 0.25 to 0.25 at intervals of 0.05. The ratio of normal wall height to arterial length is 0.06

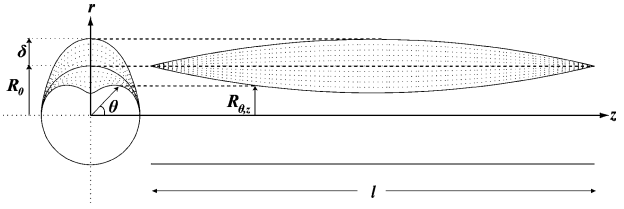

Fig. 6 Schematic diagram of a single experimental arterial segment in the $(r - z)$ and $(r - \theta)$ plane. The shape of the lesion is constructed idealistically using the shape parameters k_θ, s_θ and s_z, and dimensional parameters δ, R_0 and l. The geometrical shape may not reflect the real life structure exactly. Although multiple abnormal segments can be constructed, and flow through such a vessel can be solved, we considered only one diseased segment to simplify the study of relationship between flow resistance and lesion geometry

will cause a larger force of expansion after the flow enters the dilation. Aspirin or acetylsalicylic acid is a drug in the family of salicylates that has an anticoagulant (blood thinning) effect and is used in long-term low-doses to prevent heart attacks. The reduction in mass concentration of blood will lower the sudden blood pressure release into the dilation and therefore mitigate the extent of aneurysm. This reduction in viscosity of blood corresponds to a drop in its flow behavior index.

5.2 Effect of spiraling lesion on flow resistance

Equations 10–12 translate into a radial geometry that can be shown in cross-sectional planes cutting along the central axis of the artery. In Fig. 8, ten coronal planes of the artery are sampled to illustrate the circumferential location of the lesion as it spirals along the arterial wall length.

Figure 9 shows the surface curve of flow resistance ratio responding to the effect of radial shape parameter and degree of lesion spiraling. The shape parameter, s_θ is varied from 0.5 to 10.5 at intervals of 1.0. The number of lesions, $k_\theta = 1$, and the degree of spiral ψ along the wall of the artery varies from 90° to 360°.

The flow resistance ratio in the longitudinal flow reduces as the magnitudes of ψ and s_θ increase. The flow resistance ratios corresponding to flow behavior indices $n = 1$, $\frac{1}{2}$ and $\frac{1}{3}$ are shown by the solid, dash and dotted response surfaces respectively in Fig. 8. For the same geometrical configuration, low values of n results

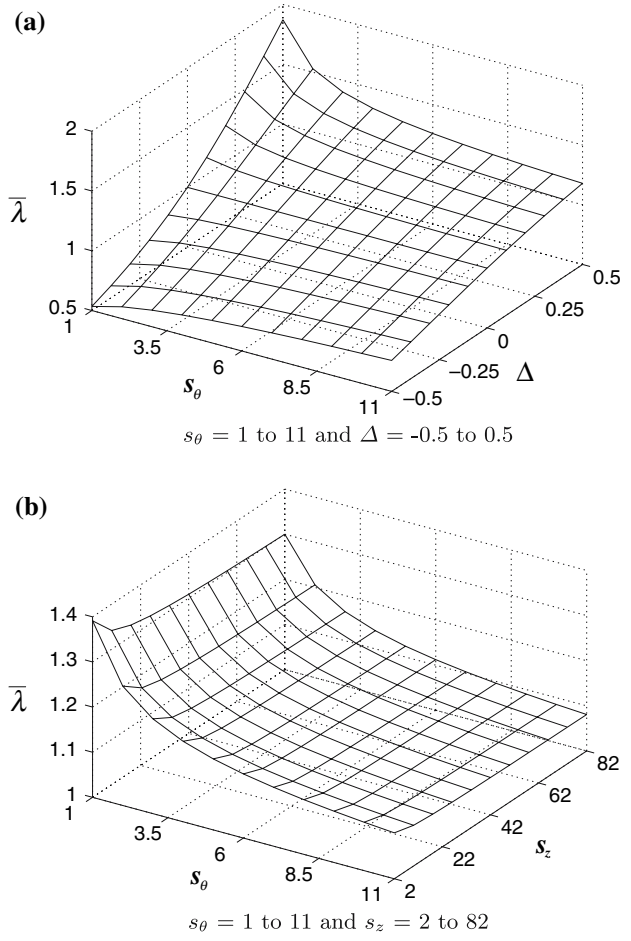

Fig. 7 Variation of flow resistance ratio $\overline{\lambda}$ for parameters Δ, s_z and s_θ. The axial shape parameter is standardized at $s_z = 2$ as s_θ and Δ vary, and the diseased height is fixed at Δ = 0.25 for the variation of s_θ and s_z. The response of $\overline{\lambda}$ to the lesion geometrical configuration can be determined mathematically. The surface response curve is able to explain the relationship between flow resistance and the geometry of the lesion clearly and effectively

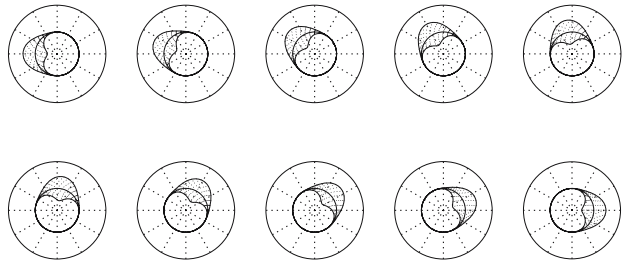

Fig. 8 Geometrical profiles of lesion along the walls of a diseased artery by a phase shift of ϕ for $\psi = 180°$ Cross-sectional views that are sliced along ten equal divisions of the arterial length from upstream to downstream of the blood flow shows the helical profile from a different perspective. The localized lesion viewed from these coronal planes is shown to rotate through an angle of 180°

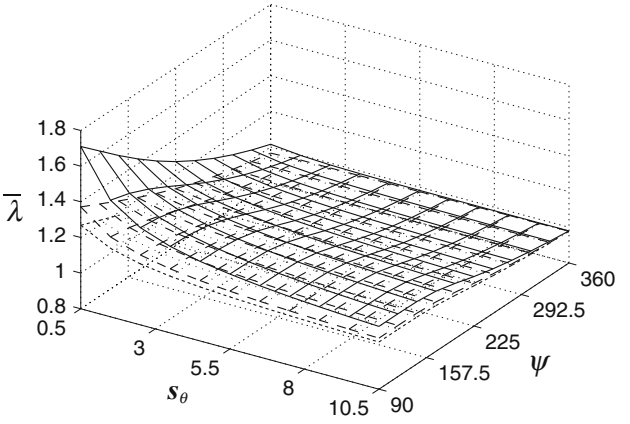

Fig. 9 Flow resistance ratio of flow through diseased artery response to s_θ = 0.5–10.5 and ψ = 90°–360°. We vary these two parameters to show how their modifications can affect lesion spiraling. The graph is effective in relating flow resistance through a diseased vessel with localized lesion arranged helically, to the degree of its spiraling. It serves as a simple mathematical tool to link parameters of interest when analyzing the flow properties, but at the expense of simplification of the model

in a smaller degree of spiraling. The spiraling of the lesion reduces blood flow resistance and the pressure build-up along the arterial wall and reduces the risk of post-stenotic aneurysm. Nevertheless, the pathological remodeling of an atherosclerotic vessel is limited by the structural integrity of the diseased segment that is dependent on the composition of the lesion and properties of the media and adventitia [36]. At any coronal cross-section and for a non-uniformly occluded artery, the cross-sectional flow is always larger than that with a uniform stenosis:

$$\int_0^{2\pi}\left(\frac{R_{z,\theta}}{R_0}\right)\mathrm{d}\theta > \int_0^{2\pi}\left(\frac{R_z}{R_0}\right)\mathrm{d}\theta. \tag{35}$$

Raising the radial dimension to a higher order and taking the reciprocal of the terms:

$$\frac{1}{\int_0^{2\pi}\left(\frac{R_{z,\theta}}{R_0}\right)^3\mathrm{d}\theta} < \frac{1}{\int_0^{2\pi}\left(\frac{R_z}{R_0}\right)^3\mathrm{d}\theta}. \tag{36}$$

Integration and raising the order of solution to n yields:

$$\overline{\tau}(z,\theta) < \overline{\tau}(z) \tag{37}$$

The wall shear stress of a spiraling lesion at any point along the arterial wall in the longitudinal direction is smaller than that of an axial symmetrical or uniformly stenotic artery. The helical lesion spreads the localized wall shear stress along a spiral path and reduces flow

resistance in the axial direction. This reduces resistance to flow and wall shear stress thus lowering the chance of rupture and thrombosis compared to that in an axially symmetric stenosis of similar height.

6 Discussion

The mathematical description of a longitudinally and circumferentially varying occlusion due to the non-uniformity of the lesion growth can be constructed based on the separation of axial and angular expressions along the z and θ directions respectively. The variation in the flow properties due to modifications in arterial profile presented in the two orientations can be represented by a three-dimensional response surface map. Useful analysis can be based on the variation profile of this surface map that determines the nature of response of the flow resistance ratio to the geometrical modifications of the artery, rather than exact values of the examined flow property for a designated arterial segment. The nature of response here refers to the polarity of change in flow resistance ratio, and the degree of response states the magnitude change in the property that is measured.

The Casson model is a more accurate model of human blood in vivo than the power law model [26]. However, the differences are small and the power law model predicts less flow than the Casson rather than more flow as is the case with Newtonian alternatives [3]. Use of the power law model has made it possible to solve for resistance to flow ratio and wall shear stress ratio through the complicated wall geometry introduced to allow more realistic modeling of actual stenotic shapes.

The use of first order instead of second order shear strain in the derivation of longitudinal flow resistance through an atherosclerotic artery is considered in this study to reduce the flow model from three-dimension to one-dimension. This is the reason that vortex and unsteady flow have not been considered. The dominant shear strain is assumed to exist along the flow direction as the only non-zero gradient component in a steady state flow condition. Although such assumptions may limit the accuracy of the flow resistance values that are based on the parameter values pertaining to every arterial configuration, the nature of the flow resistance ratio surface will be affected minimally by the components of the shear strain acting along the other planes.

The main contribution of this paper is the introduction of a more realistic wall geometry that has previously been used with analytic mathematical modeling methods. The assumption of a straight rigid arterial wall rather than a curving viscoelastic one has been necessary to simplify the problem, making it tractable. Nuances can be added to the model and it should be possible to add in curvature or even viscoelasticity if required, although this would be challenging.

7 Conclusion

Clinical interest in quantifying the reduction in flow through a coronary artery caused by a stenosis and theoretical interest in quantifying the increase in wall shear stress, brought about by the presence of a stenosis, has been frustrated through mathematical modeling traditionally focusing on very restricted stenotic geometries. We have introduced wall-modeling techniques allowing estimation of these quantities for power law flow through a lesion with complicated axial and radial variation. The mathematical model allows a better fit to real wall geometries than was previously possible through analytic techniques and uses a power law model of blood flow. Analysis of the relationships between the maximal stenotic height and the axial and radial shape parameters have demonstrated that the resistance to flow ratio is dependent on the variation of arterial wall in both the coronal and sagittal planes.

The improvements in the modeling of wall geometry have allowed consideration of spiraling stenoses in straight arteries. To be clinically relevant in the coronary arteries, this must be extended to helical stenoses in curving arteries. As they stand, the results are of interest for other arteries and are suggestive of what may be found in more realistic curving models of the coronary arteries. The introduction of a spiraling stenosis spreads the post-stenotic increase in wall pressure along the artery and should reduce the risk of post-stenotic dilatation or aneurysm.

The proposed formulation of the wall geometry is able to relate the structural profile of the transport vessel with flow properties at low computational cost and in a non-invasive manner. This has possible applications in provision of reduction of flow estimates in angiography equipment and in situations where practical experimental measurement of flow is not possible. There are some limitations in the relationship between the different non-dimensional parameters due to assumptions of idealistic blood flow behavior indices and homogenous and irrotational flow. There may also be minor accuracy problems because the arterial wall is assumed to be rigid rather than viscoelastic but previous work [32] has shown the differences to be minor in those cases that have been examined. No experimental

validation of the results has been carried out but the power law model is known to fit the behavior of blood in small arteries almost as well as the Casson model.

References

1. Ang KC, Mazumdar JN (1995) Mathematical modelling of triple arterial stenoses. Aust Phys Eng Sci Med 18:89–94
2. Aroesty J, Gross JF (1972) Pulsatile flow in small blood vessels—I, Casson Theory. Biorheology 9:33–43
3. Baaijens JP, van Steenhoven AA, Janssen JD (1993) Numerical analysis of steady generalized newtonian blood flow in a 2d model of the carotid artery bifurcation. Biorheology 30(1):63–74
4. Banerjee RK, Back LH, Back MR, Cho YI (2000) Physiological flow simulation in residual human stenoses after coronary angioplasty. J Biomech Eng 122(4):310–320
5. Berger SA., Jou LD (2000) Flows in stenotic vessels. Ann Rev Fluid Mech 32:347–382
6. Bingham E (1922) Fluidity and plasticity. MacGraw Hill, New York
7. Casson N (1959) A flow equation for pigment oil suspensions of the printing ink type, rheology of dispersive systems. In: Mills CC (ed) Pergamon press
8. Chakravarty S, Datta A (1992) Dynamic response of stenotic blood flow in vivo. Math Comput Model 16:3–20
9. Cokelet GR (1972) Biomechanics, its foundations and objectives, chap. The rheology of human blood. Prentice-Hall, pp 63–87
10. Davies, MJ (1996) Stability and instability: two faces of coronary atherosclerosis. Circulation 94:2013–2020
11. Davies, MJ, Thomas AC (1985) Plaque fissuring-the cause of acute myocardial infarction, sudden ischaemic death, and crescendo angina. Br Heart J 53(4):363–373
12. Falk E, Shah PK, Fuster V (1995) Coronary plaque disruption. Circulation 92:657–671
13. Forrester J, Young D (1970) Flow through a converging diverging tube and its implications in occulsive vascular disease– I. J Biomech 3:297–305
14. Fox B, James K, Morgan B, Seed A (1982) Distribution of fatty and fibrous plaques in young human coronary arteries. Atherosclerosis 4:337–347
15. Gertz S, Roberts WC (1990) Hemodynamic shear force in rupture of coronary arterial atherosclerotic plaques. Am J Cardiol 66:1368–1372
16. Gertz SD, Uretzky G, Wajnberg RS, Navot N, Gotsman MS (1981) Endothelial cell damage and thrombus formation after partial arterial constriction: relevance to the role of coronary artery spasm in the pathogenesis of myocardial infarction. Circulation 63:476–486
17. Glagov S, Weisenberd E, Zarins C, Kolettis RG (1987) Compensatory enlargement of human atherosclerotic coronary arteries. N Engl J Med 316:1371–1375
18. Herschel H, Bulkey R (1926) Konsistenzmessungen von gummi-benzollosungen. Koll Zeitschr 23:291–300
19. Kaazempur-Mofrad MR, Isasi AG, Younis HF, Chan RC, Hinton DP, Sukhova G, LaMuraglia GM, Lee RT, Kamm RD (2004) Characterization of the atherosclerotic carotid bifurcation using mri, finite element modeling, and histology. Ann Biomed Eng 32(7):932–946
20. Kirkeeide RL, Gould KL, Parsel L (1986) Assessment of coronary stenoses by myocardial perfusion imaging during pharmocologic coronary vascodilation. J Am Coll Cardiol 7:103–113
21. MacDonald D (1979) On steady flow through modelled vascular stenoses. J Biomech 12:13–20
22. MacIsaac AI, Thomas JD, Topol EJ (1993) Toward the quiescent coronary plaque. J Am Coll Cardiol 22:1228–1241
23. Mann JM, Davies MJ (1996) Vulnerable plaque—relation of characteristics to degree of stenosis in human coronary arteries. Circulation 94:928–931
24. Mazumdar JN (1992) Biofluid mechanics. World Scientific N. J. USA
25. Mernone AV, Mazumdar JN (2000) Biomathematical modelling of physiological fluids using a casson fluid with emphasis to peristalsis. Aust Phys Eng Sci Med. 23(3):94–100
26. Morris C, Smith C, Blackshear P (1987) A new method for measuring the yield stress in thin layers of sedimenting blood. Biophys J 52:229–240
27. Pincombe B (1998) A study of non-newtonian behaviour of blood flow through stenosed arteries. Ph.D. thesis, University of Adelaide
28. Pincombe B, Mazumdar JN (1995) A mathematical study of blood flow through viscoelastic walled stenosed arteries. Aust Phys Eng Sci Med 18:81–88
29. Pincombe, B, Mazumdar JN (1997) The effects of post-stenotic dilatations on the flow of a blood analogue through stenosed coronary arteries. Math Comput Model 25:57–70
30. Pincombe B, Mazumdar JN (1998) Herschel-bulkley and casson flow through viscoelastic walled stenosed arteries. In: Tuck EO, Stott JAK (eds) EMAC'98, The Institute of Engineers, Australia, pp 399–402
31. Pincombe B, Mazumdar JN (1998) Numerical model of power law flow through an atherosclerotic artery. In: Noye BJ, Teubner MD (eds) CTAC'97, World Scientific Press, pp 563–570
32. Pincombe B, Mazumdar JN (2002) Techniques for the study of blood flow through both constrictions and post-stenotic dilatations in arteries. Handbook of computational methods in biomaterials, biotechnology and biomedical systems. Kluwer, Dorchet
33. Poiseuille J (1836) Observations of blood flow. Ann Sci Nat STrie 5, 2
34. Reiber JHC, van der Zwet PMJ, von Land CD, Koning G, Loois G, Zorn I, van den Brand M, Gerbrands JJ (1989) Online quantification of coronary angiograms with the dci system. Medicamundi 34:89–98
35. Rodbard S, Ikeeda K, Montes M (1967) An analysis of mechanisms of post stenotic dilation. Angiology 18:349–367
36. Seo HS, Lombardi DM, Polinsky P, Powell-Braxton L, Bunting S, Schwartz SM, Rosenfeld ME (1997) Peripheral vascular stenosis in apolipoprotein e-deficient mice: potential roles of lipid deposition. Medial atrophy, and adventitial inflammation. Arterioscler Thromb Vasc Biol 17:3593–3601
37. Shukla JB, Parihar RS, Rao BRP (1980) Effects of stenosis on non-newtonian flow in an artery. Bull Math Biol 42:283–294
38. Tang D, Yang C, Zheng J, Woodard PK, Sicard GA, Saffitz JE, Yuan C (2004) 3d mri-based multicomponent fsi models for atherosclerotic plaques. Ann Biomed Eng 32(7):947–960
39. Wensing JW, Meiss L, Mali PTM, Hillen B (1998) Early atherosclerotic lesions spiraling through the femoral artery. Arterioscler Thromb Vasc Biol 18:1554–1558
40. Wong KKL, Mazumdar JN, Abbott D (2005) A study of relationship between geometrical variation of atherosclerotic arteries and flow resistance. In: 12th International conference on biomedical engineering. CD only
41. Worthley SG, Helft G, Fuster V, Fayad ZA, Fallon JT, Osende JI, Roque M, Shinnar M, Zaman AG, Rodriguez OJ (2000) High resolution ex vivo magnetic resonance imaging

of in situ coronary and aortic atherosclerotic plaque in a porcine model. Atherosclerosis 150(2):321–329
42. Worthley SG, Helft G, Fuster V, Zaman AG, Fayad ZA, Fallon JT, Badimon JJ (2000) Serial in vivo mri documents arterial remodeling in experimental atherosclerosis. Circulation 101(6):586–589
43. Worthley SG, Omar-Farouque HM, Helft G, Meredith IT (2002) Coronary artery imaging in the new millennium. Heart Lung Circ 11(1):19–25
44. Young D (1968) Effect of a time dependent stenosis on flow through a tube. J Eng Ind Trans Am Soc Mech Eng 90: 248–254
45. Zohdi TI (2005) A simple model for shear stress mediated lumen reduction in blood vessels. Biomech Model Mechanobiol 4(1):57–61